Supplemental Material

Body Surface and Intracardiac Electrograms

T-wave alternans (TWA) estimates were obtained from the two body surface leads, 12 intracardiac unipolar leads (three in each of the right-ventricular, left-ventricular, and coronary sinus catheters) seen in Figure OS1.

Figure OS2 shows representative examples of body surface and intracardiac electrograms obtained prior to R-wave triggered pacing. These electrograms demonstrate that all catheter leads provide artifact-free and high-fidelity signals with high signal to noise ratio, appropriate for the TWA analysis.

Delineation of the T-wave Boundaries Using the Wavelet Transform

The first step in the phase analysis involves the robust estimation of the T-wave boundaries. Considering the variability in the morphology as well as the timing of the T-wave among different leads, the T-wave boundaries were independently determined on a beat-by-beat basis for each of the body-surface and intracardiac leads. Therefore, we developed a software-based T-wave delineation algorithm. This method is an updated version of the previously developed technique for surface ECG delineation based on the wavelet transform (WT) [1].

The wavelet transform provides a multi-resolution decomposition of the signal as a combination of a set of basis functions, obtained by means of dilation and translation of a single prototype function, namely the mother wavelet [2]. It is possible to identify the significant points of the ECG signal using the information of local maxima, minima and zero crossings of the WT coefficients at different scales.

Briefly, for each beat, the dyadic wavelet transform of the signal was estimated using a quadratic spline wavelet for the first five scales, wherein most of the energy of the signal lies. We obtained QRS complex annotations (QRS onset, Q, S and QRS offset) by the zero crossing detection of the wavelet coefficients between a positive maximum-negative minimum pair at the first scale, which corresponds to the highest frequency component of the ECG beat. Afterwards, a search window relative to the R position and depending on the RR interval was defined. Within this window, the maximum modulus of WT in scale 2^4 was computed, based on which we

assigned one out of six possible morphologies to the T-wave as positive, negative, positive-negative biphasic, negative-positive biphasic, ascending and descending [1].

It is noteworthy that the presented WT algorithm can be applied directly over the raw ECG signal without any pre-processing. In fact, the frequency domain filtering is implicitly performed when computing the WT, eliminating the need to pre-filtering the digitized signal and allowing the direct application over the raw data.

T-wave Alternans Estimation Algorithm

We employed a previously described alternans analysis algorithm [3,4] for the estimation of intracardiac TWA.

Preliminary R-wave time points were obtained by applying a software-based QRS detection algorithm to surface electrogram lead V4. Then, QRS detections were refined and abnormal beats, for example, premature ventricular complexes (PVCs) and aberrantly conducted beats were identified using a template-matching QRS algorithm [3]. Briefly, for each new beat, an 80-ms window centered at the peak of the QRS complex was formed from the preliminary beat detection; an isoelectric PR segment was automatically subtracted as a zero amplitude reference point (by estimating the mean voltage in a 10-ms window preceding the start of each QRS complex). A median QRS template was generated from all "normal" QRS complexes across the previous 127 beats, and the beat was aligned to the QRS template using cross-correlation. Cross-correlation was repeated twice for each new QRS complex to ensure proper QRS alignment. A beat was considered "abnormal" if its correlation coefficient was less than a threshold value of 0.95 or if the preceding R-to-R (R-R) interval was at least 10% shorter than the mean R-R interval of the previous 7 beats. Once all abnormal beats were identified in a 128-beat sequence, each abnormal beat was substituted with a median odd or even template beat on a lead-by-lead basis (derived from the odd or even "normal" beats respectively in the 128-beat sequence), depending on whether the abnormal beat was an even or odd beat.

Then, delineation of the T-wave boundaries (T_{onset}, T_{offset}) was performed using the wavelet transform, as described above. Spectral alternans analysis was performed on a beat-by-beat basis for each 128-beat data sequence using a 512-point power spectrum to improve the frequency-domain resolution. To account for the spatial variability of TWA, spectral analysis was independently performed for each lead. Repolarization alternans indices were estimated as follows:

$$\text{alternans voltage } (\mu V) = \sqrt{\text{alternans peak} - \mu_{noise}}$$

$$K_{score} = \frac{\text{alternans peak} - \mu_{noise}}{\sigma_{noise}}$$

where, the alternans peak is the peak in the aggregate power spectrum corresponding to 0.5 cycles/beat and the mean (μ_{noise}) and the standard deviation (σ_{noise}) of spectral noise are estimated from a predefined aggregate power spectrum noise window (0.40-0.46 cycles/beat). The alternans voltage is a direct measure of the presence of alternans while the alternans K_{score} is a measure of the statistical significance of the alternans voltage. For each lead, alternans was estimated on a beat-by-beat basis using a rolling 128-beat window that was shifted one beat at a time.

Signal Processing Methods

To quantitatively investigate the degree of synchronous alternation between two waveforms, the coherence of two signals (x[n] and y[n]) has been estimated using the Welch's averaged periodogram method [5]. The magnitude squared coherence is defined as the ratio of the power spectral densities of signals x[n] and y[n] to the cross power spectral density of x[n] and y[n]. The cross-spectral density indicates the part of y[n] that is linearly related to x[n] as a function of frequency, or alternatively it can be interpreted like the cross-correlation function except it provides the expected results as a function of frequency. The coherence estimate is a function of frequency with values between 0 and 1 that indicates how well y[n] corresponds to x[n] at each frequency (0/1 indicating the lowest/highest coherence); in the case of T-wave alternans, we focus on the coherence values at 0.5 cycles/beat.

In order to detect TWA phase resetting, we estimated the cross-correlation of the estimated phase of TWA with the reference phase-index sequence which at the point of phase resetting, results in a zero-crossing of the correlation coefficient and a change in the polarity of the correlation coefficient in the vicinity of the zero crossings.

Triggered Pacing Induced TWA in the Normal Heart

R-wave triggered pacing during the absolute refractory period was used to induce alternans in the normal heart.

Pacing pulses were delivered on every other beat basis from two leads (RV12) of a decapolar catheter at the apex of the RV. We used pacing pulses of (i) amplitude: ±1 mA and ±5 mA, (ii) width: 30 ms and (iii) coupling to the R-wave: 10 ms. Figure OS3 demonstrates the K_{score} for a single subject before and after R-wave triggered pacing (initiated at beat #177), for body-surface, CS, LV and RV leads. The increase in K_{score} suggests the ability to modulate ventricular repolarization and induce TWA.

Detection of TWA Phase Resetting

Having examined the ability of the proposed method to estimate the phase of TWA, we evaluated the use of the PI as a means to detect phase resetting (Figure OS4). In order to detect potential TWA phase resetting, we estimated the cross-correlation of the estimated TWA phase with that of the reference phase-index sequence, which at the point of phase resetting is expected to result in a zero-crossing and a change in the polarity of the correlation coefficient.

We generated an N point time series of an ideal alternating phase-index. Two phase resetting points were introduced into this sequence by reverting the PI at two different pre-specified points, i=70 and j=130. An M-point (M=36) running window was used to estimate the cross correlation with the reference alternating time series. In computer simulated data (Figures OS4, panels A and B), we demonstrate that in the presence of phase resetting, the cross correlation of the phase index changes from 1 to -1 (or vice versa), crossing the zero point at the phase resetting point. The transient decrease/increase starts M/2 points before the phase resetting point and lasts for M/2 points after the phase resetting point. The change in the polarity of the estimated cross correlation in the M-point window is used to determine the phase resetting location at the zero crossing point.

Phase-Dependent Coherence Estimation During R-wave Triggered Pacing

In Figure OS5, we show the phase coherence variation as a result of applying R-wave triggered pacing pulses to induce and suppress TWA from two catheter leads in the RV (induction lead: RV12; suppression lead: RV34; pulse amplitude: -7mA; pulse width: 30ms; coupling to R-wave: 30ms).

Intervention A shows that the level of coherence in the presence of atrial pacing (100 bpm), is low. Intervention B demonstrates a significant rise in the coherence (due to an increase in the alternans voltage and K_{score}) resulting from R-wave triggered pacing from RV12 on an every even beat basis. In intervention C, triggered pacing continues from RV12 on even beats, however, triggered stimuli are now delivered from RV34 on every odd beat, and the

coherence substantially decreases (due to a decrease in the alternans voltage and K_{score}) because the distinction between odd and even beats is essentially lost by delivering R-wave triggered pacing pulses during each beat. In intervention D, R-wave triggered pacing continues from RV12 on every even (-7 mA) and from RV34 on every odd beat; however, the polarity of the pacing stimulus delivered on each odd beat from RV34 is reversed (+7 mA). Reversing the polarity of RV34 results in a significant increase in the coherence (due to an increase in the alternans voltage and K_{score}) because the opposite polarity pacing pulses accentuate the distinction between odd and even beats. In the following intervention (E), R-wave triggered pacing from RV12 continues on every even beat (-7 mA) but triggered pacing is now delivered from RV34 also on every even beat but with an opposite polarity pulse (+7 mA). Finally, in intervention G, the coherence again decreases (due to a decrease in the alternans voltage and K_{score}) during triggered pacing from RV12 on every even beat because the distinction between odd and even beats is eliminated. Thus, lack of a priori knowledge of the phase of TWA may result in an increase in the TWA amplitude (as shown in interventions B, D and F). Therefore, in order to effectively suppress TWA, one needs to know the phase of the estimated TWA.

ECG Morphology Changes During TWA Suppression in the Presence of Acute Ischemia

In Figure 6 of the manuscript we present the utility of phase-dependent R-wave triggered pacing during the absolute refractory period to suppress spontaneous TWA.

In Figure OS6, we present the change of ECG morphology from baseline in sinus rhythm (when significant TWA is present), to TWA suppression by pacing during the absolute refractory period (one may see the pacing pulse and appreciate that the discrimination of even/odd beats is lost) and back to baseline (when significant TWA is manifested again). In Figure OS6, the median odd/even beats (in a 128-beat sequence) of the triangular intra-cardiac bipolar lead configuration CS2CS8, CS2LV4 and CS2LV10 are shown during spontaneous TWA (intervention A), in-phase R-wave triggered pacing with positive pulse polarity (intervention B) and baseline TWA (intervention C). While we observe visible TWA in both baselines (interventions A and C), intervention B demonstrates a significant reduction in the alternans level, to the extent that TWA is no longer visible.

Online Supplement Figure Captions

Figure OS1 Typical catheter position in the right ventricle (RV), left ventricle (LV), coronary sinus (CS) and right atrium (RA).

Figure OS2 Representative electrograms from surface lead V4 and unipolar intracardiac leads from Coronary Sinus (CS), Left Ventricular (LV) and Right Ventricular (RV) catheters with reference to an electrode in the inferior vena cava. The amplitudes of signals have been normalized.

Figure OS3 Repolarization alternans induction following R-wave triggered pacing on every other beat during absolute refractory period in the normal heart. K_{score} is plotted for a body-surface lead (ECGII), one CS lead (CS1U), one LV lead (LV9U) and one RV lead (RV3U) from a single study subject. There is a significant increase in K_{score} after the onset of R-wave triggered pacing during the absolute refractory period (initiated at beat no 177). The TWA increase in RV lead is more profound due to its proximity to the pacing site.

Figure OS4 Use of phase estimation to detect phase resetting. (A) Computer simulated data indicate two examples of phase resetting, at points i=70 and j=130. (B) Detection of the phase resetting points using the cross-correlation of the simulated data shown in (A) with the reference phase using an M-point (M=36) running window.

Figure OS5 Phase-dependant average coherence in body-surface leads, and intracardiac CS, LV and RV leads resulting from RV12 and RV34 ventricular triggered pacing (amplitude: -7 mA; pulse width: 30 msec; coupling to R-wave: 30 msec) in the presence of atrial pacing at 100 bpm. The following pacing interventions were performed from the pacing leads: **A**: baseline, atrial pacing only, **B**: RV12 every even beat, **C**: RV12 every even & RV34 every odd beat, **D:** RV12 every even beat (-7 mA) & RV34 every odd beat but with the opposite polarity current pulse (7 mA), **E:** RV12 every even (-7 mA) & RV34 every even beat but with the opposite polarity current pulse (7 mA), **F**: RV12 every even beat & RV34 every even beat, **G**: RV12 every beat.

Figure OS6 ECG morphology changes during spontaneous TWA suppression in the presence of acute ischemia. Intervention A: visible TWA in sinus rhythm following coronary artery balloon occlusion; Intervention B: in-phase triggered pacing with positive pulse polarity delivered from

RV12 on every even beat decreases alternans level; Intervention C: R-wave triggered pacing is discontinued and TWA becomes visible during sinus rhythm. Panels show the median odd(red)/even(blue) beats in a 128-beat sequence of the triangular intra-cardiac bipolar lead configuration CS2CS8, CS2LV4 and CS2LV10 during each intervention.

References

1. Martínez JP, Almeida R, Olmos S, Rocha AP, Laguna P. A Wavelet-Based ECG Delineator: Evaluation on Standard Databases. *IEEE Trans. Biomed.* 2004;51(4):570-581.

2. Mallat S. A theory for multiresolution signal decomposition : the wavelet representation. *IEEE, Transaction on Pattern Analysis and Machine Intelligence.* 1989;11:674-693.

3. Weiss EH, Merchant FM, d'Avila A, Foley L, Reddy VY, Singh JP, Mela T, Ruskin JN, Armoundas AA. A novel lead configuration for optimal spatio-temporal detection of intracardiac repolarization alternans. *Circ Arrhythm Electrophysiol.* Jun 1, 2011: 407-417.

4. Armoundas AA, Weiss EH, Sayadi O, Laferriere S, Sajja N, Mela T, Singh JP, Barrett CD, Heist EK, Merchant FM. A Novel Pacing Method to Suppress Repolarization Alternans in Vivo: Implications for Arrhythmia Prevention. *Heart Rhythm (In Press).* 2012.

5. Bendat JS, Piersol AG. *Engineering applications of correlation and spectral analysis*. 1st ed. New York: John Wiley and Sons, Inc; 1980.

Online Supplement Figure 1

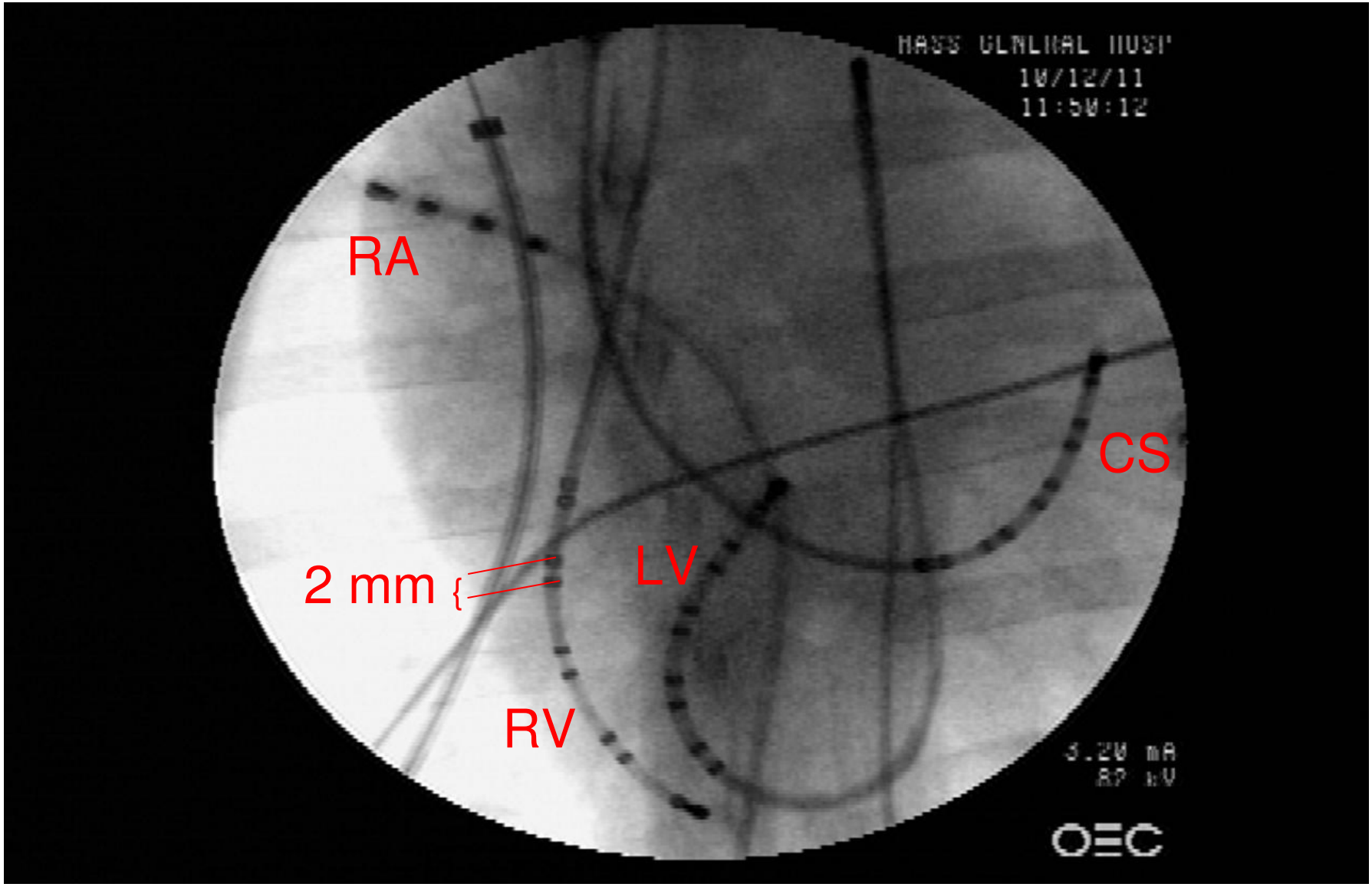

Online Supplement Figure 2

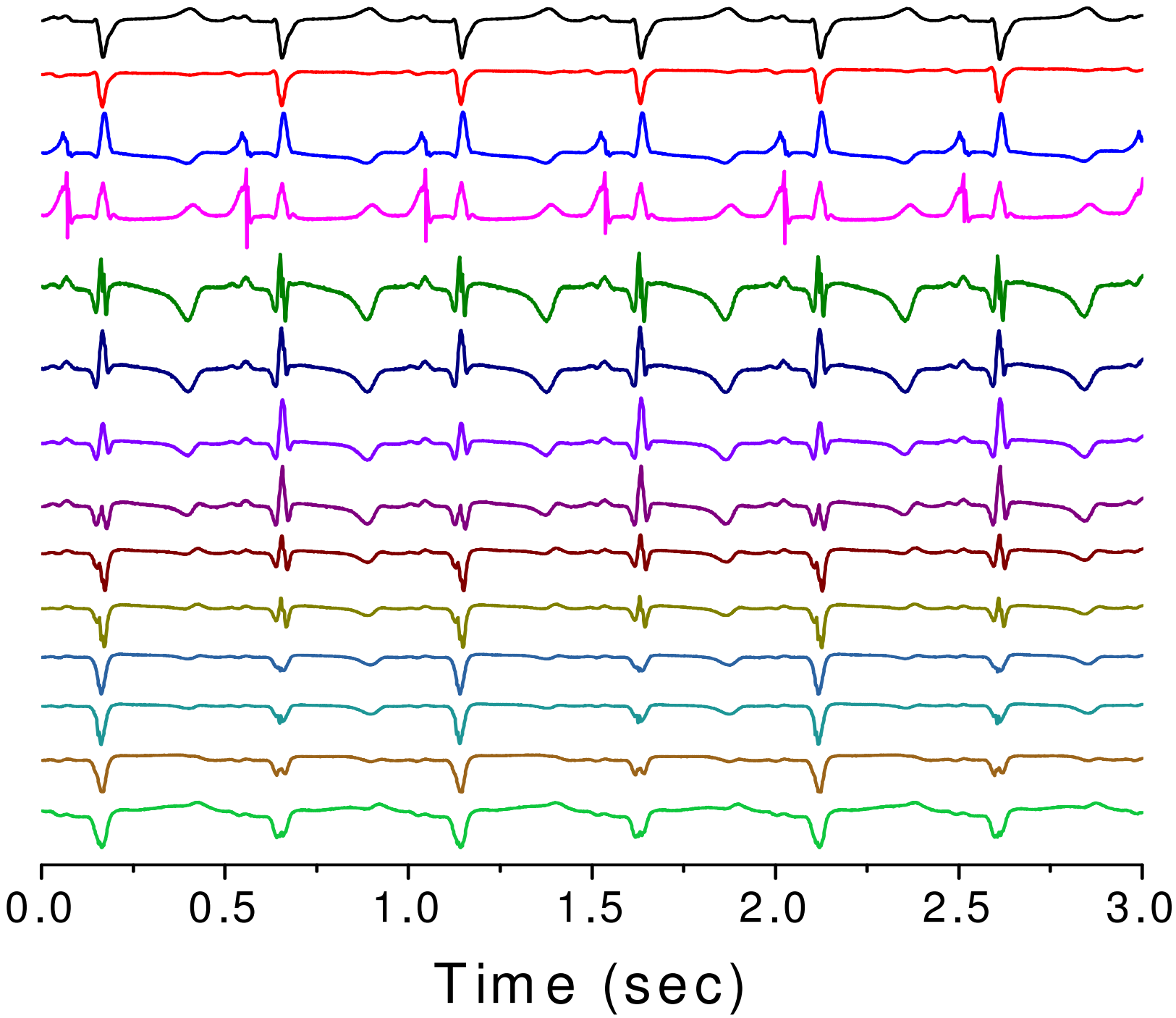

Online Supplement Figure 3

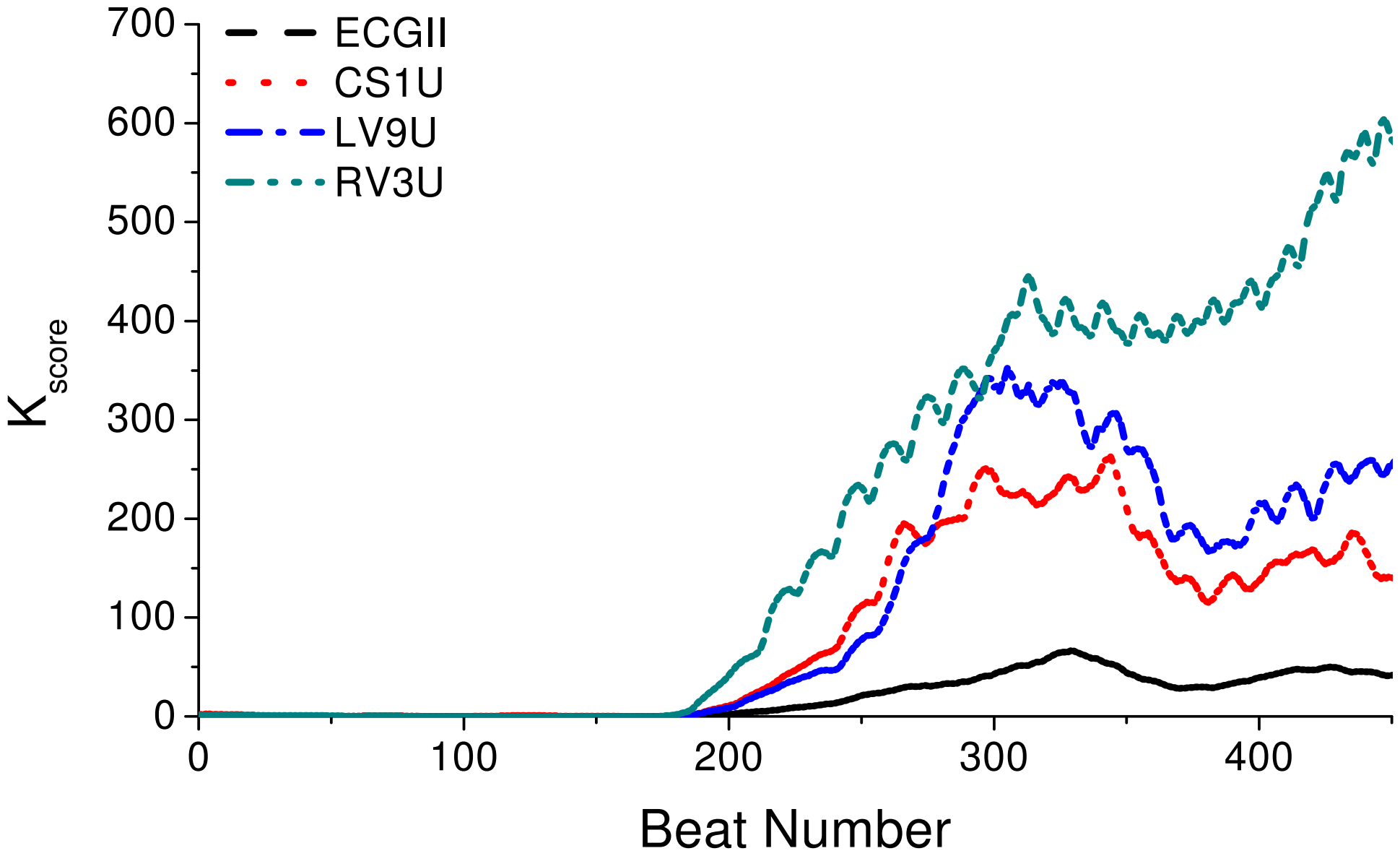

Online Supplement Figure 4

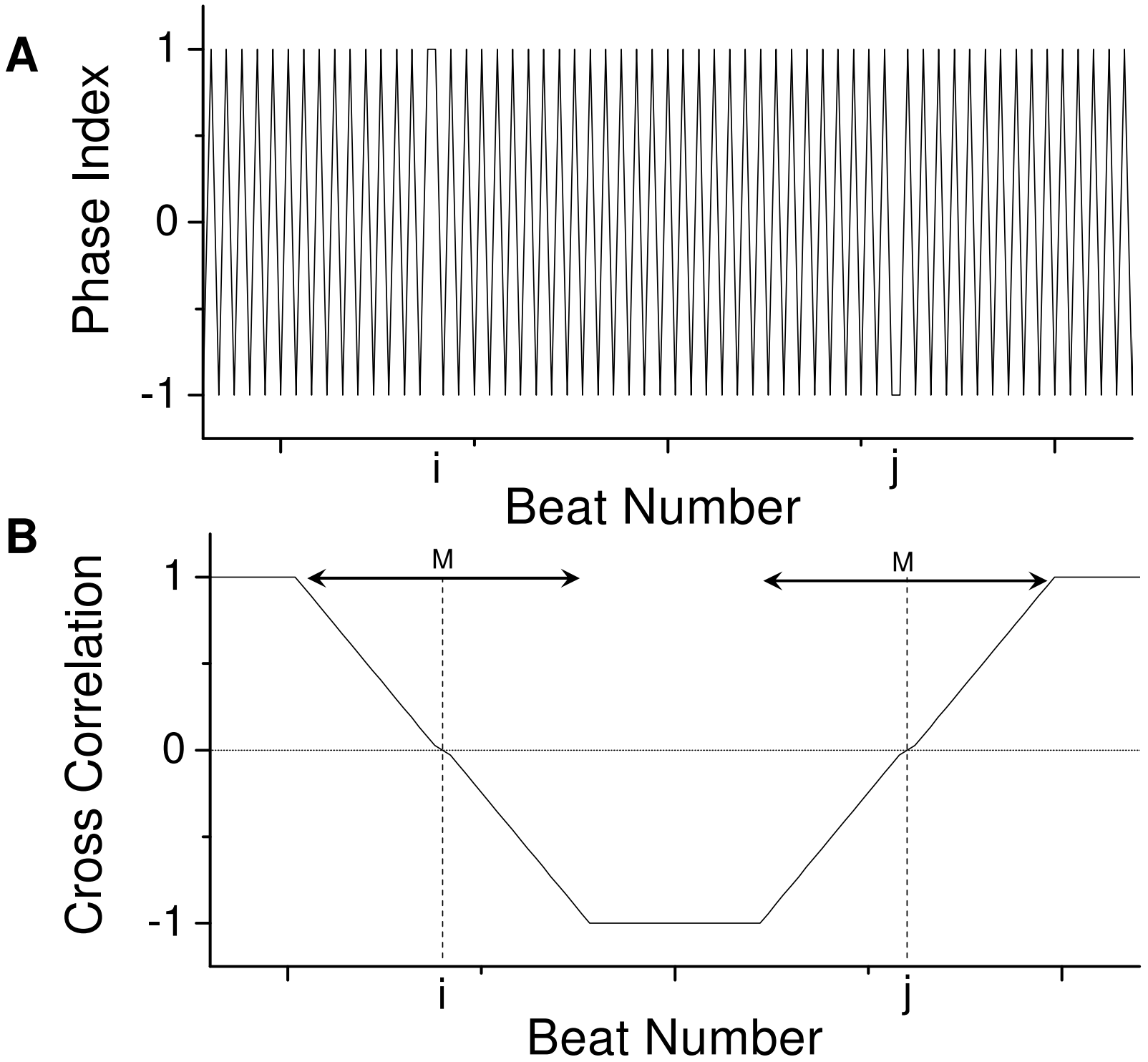

Online Supplement Figure 5

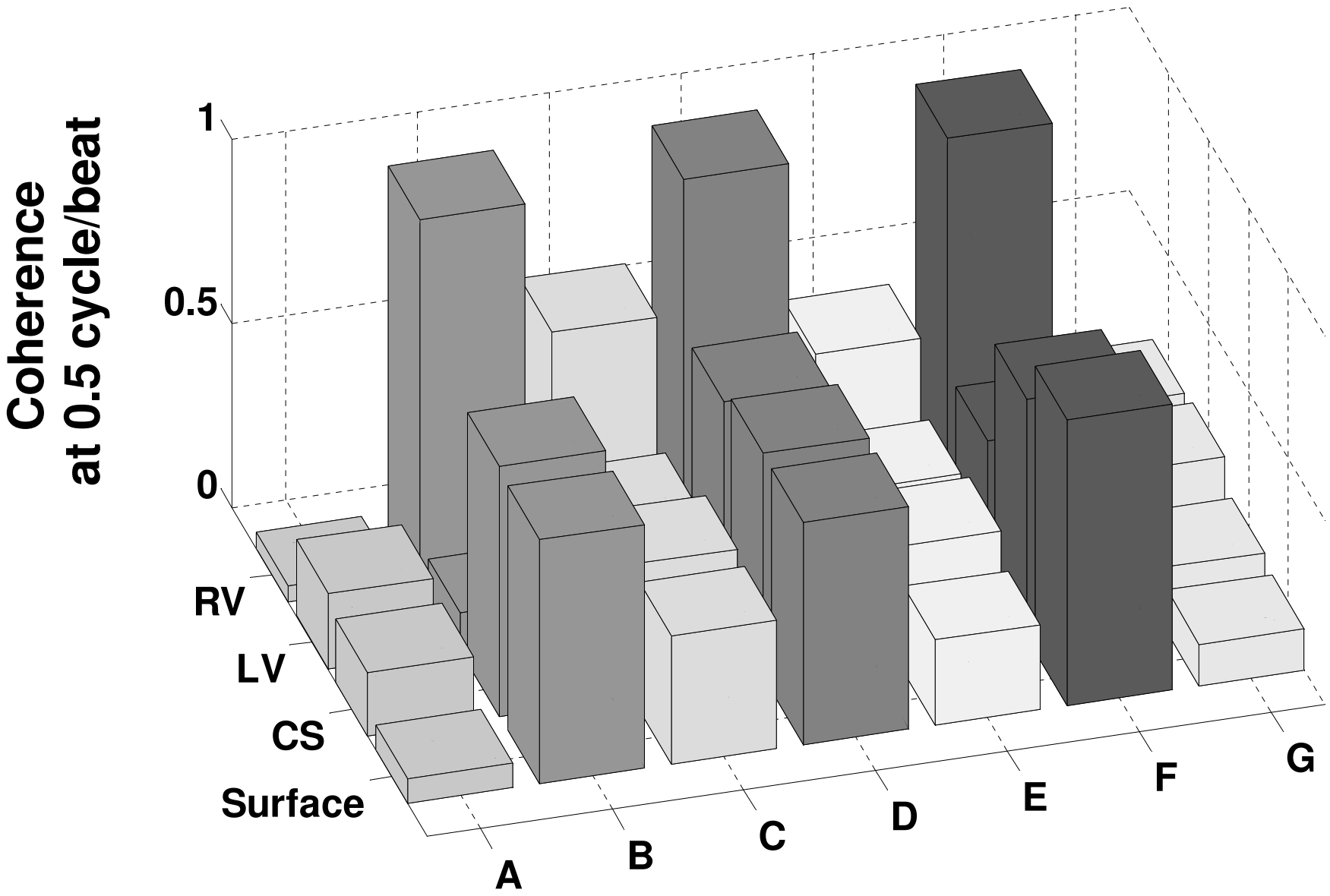

Online Supplement Figure 6